ACROSS
Journal of Interdisciplinary Cross-Border Studies
Vol 9, No.1, 2025

Laminate architecture effects on three-point bending performance of textile-reinforced epoxy composites

Vasile BRIA*, Marina BUNEA*

*"Dunărea de Jos" University of Galați, Romania

Abstract

In this study, we aim to identify the correlation between the architecture of the manufactured materials and the three-point bending mechanical behavior of laminated composite materials with a thermoset polymer matrix. The composites were fabricated under controlled laboratory conditions using an epoxy system consisting of Epyphen DE4020 resin and Epyphen RE4020 hardener and were reinforced with woven glass fiber and carbon fiber fabrics. For each material category, five distinct laminate architectures were designed by varying the angular orientation of thirteen plies, ranging from unidirectional and cross-ply configurations to discrete and progressive multiaxial layouts.
Rectangular specimens with a width of 15 mm, a length of 110 mm, and variable thicknesses were extracted from the manufactured laminates and subjected to three-point bending tests with a support span of 64 mm, in accordance with ASTM D5023–99(01), Standard Test Method for Measuring the Dynamic Mechanical Properties of Plastics Using Three-Point Bending in Flexure. The parameters determined included the flexural modulus, energy at the elastic limit, load at the elastic limit, stress at the elastic limit, energy to fracture, load at fracture, and stress at fracture. The experimental data were statistically processed using a robust methodology based on the interquartile range (IQR) and the median absolute deviation (MAD) to eliminate aberrant values and to compute refined representative mean values.

Keywords: Laminated composite materials; laminate architecture; carbon fiber; glass fiber; epoxy matrix; flexural mechanical properties.

Introduction

Laminated composite materials reinforced with continuous fiber textiles have become a reference class of structural systems in aerospace, automotive, energy, and defense applications due to their favorable combination of high specific stiffness, mechanical strength, energy absorption capability, and architectural design flexibility. In these systems, the global mechanical response is not governed solely by the intrinsic properties of the fibers and the polymer matrix, but fundamentally by the laminate architecture, defined by the fabric type, the angular orientation of the plies, and the stacking sequence, which control load transfer mechanisms as well as the initiation and propagation of damage at both micro- and macrostructural scales.

Recent studies have shown that tailoring laminate architecture enables directional control of stiffness and mechanical behavior under complex loading conditions. For example, in (Al-Nadhari, Ulus and Topal, 2025), the authors demonstrated through a multi-instrumental approach that the use of hybrid glass–aramid textiles in three-dimensional woven structures leads to significant stiffness variations under tensile and shear loading, highlighting the critical role of composite architecture in strain field distribution. Similarly, in (Bao et al.,

2022), the authors reported that carbon/aramid hybrid woven composites, through controlled ply orientation, influence both conventional mechanical properties and the ballistic response of composite structures.

An essential aspect in the design of textile-reinforced composites is the anisotropy induced by fiber orientation and fabric geometry. In (Gonabadi et al., 2022), the authors showed, using full-field strain measurement techniques and multiscale modeling, that angular variations in glass fiber-reinforced polymer laminates lead to non-uniform stress distributions and pronounced differences in tensile and shear behavior (Ungureanu and Bria, 2022). Converging results are also reported in (Kostunin et al., 2016), (Zhou et al., 2021), where the mechanical anisotropy of nanomodified carbon fiber-reinforced composites was analyzed, emphasizing the influence of fabric architecture on directional stiffness and damage mechanisms.

From the perspective of dynamic loading and energy absorption capacity, composite architecture plays a dominant role in controlling failure modes. Bergmann *et al.* in (Bergmann, Heimbs and Maier, 2015) investigated the off-axis tensile behavior of woven fabric composites and showed that ±45° orientations activate interlaminar shear mechanisms that enhance energy dissipation (Capatina et al., 2019). In an applied context, Hu *et al.* in (Hu et al., 2016) demonstrated that fiber orientation in glass cloth/epoxy composite tubes significantly affects collapse modes and the absorbed energy under quasi-static axial loading and impact conditions.

In parallel, considerable attention has been devoted to hybrid composites and alternative textile reinforcements, such as aramid, basalt, jute, and flax, as strategies to optimize the balance between mechanical performance and sustainability. Sarasini *et al.* in (Sarasini et al., 2013) analyzed the residual flexural behavior of aramid/basalt hybrid composites after impact, highlighting how laminate architecture governs the retention of structural stiffness. Related findings were reported by Yahaya *et al.* in (Yahaya et al., 2016) and Manohar *et al.* in (Manohar et al., 2020), who showed that fiber orientation and textile type lead to significant variations in the mechanical properties of composites intended for protective and structural applications.

Although the literature provides a solid foundation regarding the influence of composite architecture on tensile, shear, impact, and fatigue behavior, systematic studies directly correlating laminate architecture with three-point bending performance in epoxy-based woven glass fiber and carbon fiber composites remain limited, particularly with respect to progressive multiaxial configurations and the application of robust statistical post-processing of experimental data (Bunea et al., 2021).

Materials and testing procedure

Materials

The ten composite materials investigated in this study were manufactured by layer-by-layer lay-up (manual lamination) of glass fiber woven fabrics and carbon fiber woven fabrics, impregnated with a two-component epoxy system consisting of Epyphen DE4020 resin and Epyphen RE4020 hardener. For each material, a specific laminate architecture was defined by the angular orientation sequence of the plies and their distribution with respect to the mid-plane of the laminate.

The textile reinforcements were selected to ensure uniform impregnation and effective interfacial adhesion with the epoxy matrix, aiming to obtain homogeneous laminates with reduced porosity and reproducible mechanical properties. The epoxy system was chosen due to its chemical and mechanical stability, high compatibility with both glass and carbon fibers, and its ability to ensure efficient load transfer between the reinforcement and the matrix.

Table 1 Properties of the glass and carbon fiber woven fabrics.

Property	Value	Value
Fabric Type	Plain weave, Silane	Plain weave
Structure	100% glass	100% carbon
Fiber Type	EC 9 - 33×2 tex	Carbon AKSACA™ A-38, 200 tex (3k)
Warp fibers / cm²	12	4
Weft fibers / cm²	2	4
Areal density [g/m²]	163	160
Thickness [µm]	120	260
Resin consumption [g/m²]	128	193

Laminate architecture and ply configuration

For each material category, five distinct laminate architectures were designed, each laminate consisting of thirteen plies oriented at predefined angles with respect to the longitudinal direction of the specimen. The architectures were conceived to cover a wide range of mechanical behaviors, from unidirectional configurations to progressive multiaxial structures, in order to evaluate the influence of angular distribution on flexural stiffness and strength.

The angular orientations of the plies for each material are presented in Table 2.

Table 2 Ply orientation sequence (°) and average laminate thickness for the investigated materials

Material	Ply 1	Ply 2	Ply 3	Ply 4	Ply 5	Ply 6	Ply 7	Ply 8	Ply 9	Ply 10	Ply 11	Ply 12	Ply 13	Composite Thickness [mm]
1S	0	0	0	0	0	0	0	0	0	0	0	0	0	2.02
2S	0	90	0	90	0	90	0	90	0	90	0	90	0	2.14
3S	0	45	90	45	0	45	90	45	0	45	90	45	0	2.02
4S	0	30	60	90	-60	-30	0	30	60	90	-60	-30	0	2.06
5S	0	15	30	45	60	75	90	-75	-60	-45	-30	-15	0	2.11
1C	0	0	0	0	0	0	0	0	0	0	0	0	0	2.57
2C	0	90	0	90	0	90	0	90	0	90	0	90	0	2.72
3C	0	45	90	45	0	45	90	45	0	45	90	45	0	2.6
4C	0	30	60	90	-60	-30	0	30	60	90	-60	-30	0	2.6
5C	0	15	30	45	60	75	90	-75	-60	-45	-30	-15	0	2.5

All laminate architectures were designed as symmetric lay-ups with respect to the mid-plane, in order to minimize bending–twisting coupling effects and to ensure a stable mechanical response during three-point bending tests.

Composite manufacturing procedure

The laminates were fabricated under controlled laboratory conditions using a manual lay-up technique. Each fabric ply was individually immersed in the epoxy resin Epyphen DE4020 mixed with the Epyphen RE4020 hardener according to the manufacturers recommended mixing ratio, and then placed onto the forming surface following the predefined angular sequence.

After the placement of each ply, light pressure was applied to remove entrapped air and to ensure uniform distribution of the matrix throughout the laminate structure. Upon completion of the lay-up process, the stacked laminate was subjected to consolidation and curing at ambient temperature, followed by a post-curing thermal treatment to stabilize the mechanical properties and reduce residual stresses.

Specimen preparation

From the manufactured laminate plates, rectangular specimens were extracted by high-pressure waterjet cutting, a method selected to minimize thermal and mechanical effects on the cut edges and to reduce the risk of inducing cracks, delaminations, or structurally affected zones in the vicinity of the cutting surfaces.

The specimens were fabricated with a nominal width of 15 mm, a length of 110 mm, and variable thicknesses corresponding to each laminate architecture. Thickness measurements were performed using a digital caliper with a resolution of **0.01 mm**. After cutting, the specimen edges were visually inspected and, when necessary, lightly finished to remove local imperfections and to reduce stress concentrations that could influence the flexural test results.

Three-point bending test procedure

Mechanical testing was conducted using a three-point bending configuration on a universal testing machine, in accordance with ASTM D5023–99(01), Standard test method for measuring the dynamic mechanical properties of plastics using three-point bending in flexure. The specimens were positioned on two cylindrical supports with a span length of 64 mm, and the load was applied at the midpoint of the span, perpendicular to the plane of the laminate.

During testing, the applied force and the displacement at the loading point were continuously recorded. The following characteristic parameters were determined: flexural modulus, energy at the elastic limit, load and stress at the elastic limit, energy to fracture, load and stress at fracture.

Statistical data processing

To ensure the validity and representativeness of the experimental results, the data obtained from the testing of each material were subjected to a robust statistical post-processing procedure. The identification and elimination of outliers were performed using a combined methodology based on the interquartile range (IQR) and the median absolute deviation (MAD). Refined mean values were calculated only after excluding measurements that simultaneously exceeded the thresholds defined by both statistical criteria.

This approach reduced the influence of local manufacturing defects and experimental errors on the interpretation of the relationship between laminate architecture and the flexural behavior of the composite materials.

Experimental Results and Discussion

Overview of the Experimental Results

The statistically refined mean values obtained from the three-point bending tests for the ten laminate architectures are summarized in Table 2. The analyzed parameters include the flexural modulus, energy at the elastic limit, load and stress at the elastic limit, as well as the energy, load, and stress at fracture. The reported values were obtained through a robust statistical post-processing methodology based on the interquartile range (IQR) and the median absolute deviation (MAD), in order to ensure representativeness and to minimize the influence of aberrant measurements.

For the glass fiber-reinforced composite series (1S–5S), the flexural modulus ranges between 15.1 and 17.7 GPa, whereas for the carbon fiber-reinforced series (1C–5C) it varies between 21.5 and 32.8 GPa, highlighting a systematic stiffness contrast induced by the type of reinforcement.

Table 3 Refined mean flexural properties of glass and carbon fiber - reinforced epoxy composites under three - point bending.

Material	Modulus [MPa]	Elastic limit			Fracture		
		Energy [J]	Load [N]	Stress [MPa]	Energy [J]	Load [N]	Stress [MPa]
1S	17153	0.863	421	385	1.349	119	108
2S	16915	1.005	468	398	1.443	126	108
3S	15122	1.169	476	392	1.574	207	170
4S	17736	1.172	443	422	1.635	220	213
5S	15547	1.166	417	349	1.712	193	162
1C	23670	1.136	903	465	1.536	184	95
2C	32845	0.923	955	496	1.792	403	210
3C	30478	1.175	1206	582	1.764	401	185
4C	25182	1.063	1065	453	1.551	572	245
5C	21491	0.965	825	386	1.492	433	203

Flexural modulus analysis

The flexural modulus values shown in Figure 1 indicate a pronounced influence of both fiber type and laminate architecture on structural stiffness. Carbon fiber-reinforced composites consistently exhibit higher modulus values than glass fiber-reinforced counterparts, due to the intrinsically higher elastic modulus of carbon fibers and the more efficient load transfer at the fiber–matrix interface.

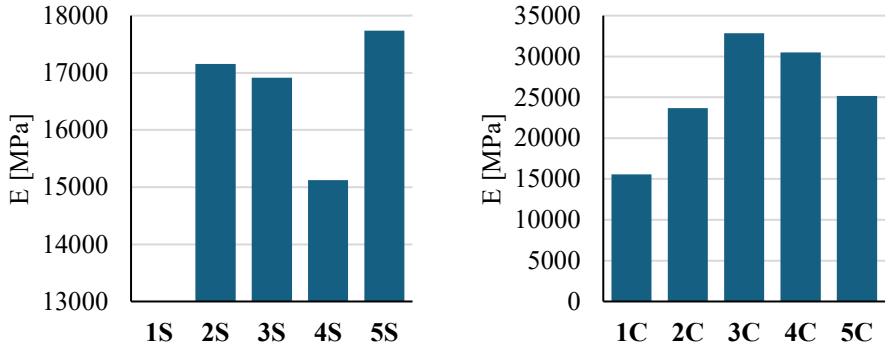

Figure 1 Flexural modulus of glass fiber (left) - and carbon fiber (right) -reinforced composites as a function of laminate architecture.

Within the glass fiber series, the highest modulus is recorded for the 4S architecture (17,736 MPa), followed by 1S (17,153 MPa) and 2S (16,915 MPa). This trend suggests that a discrete angular distribution involving plies oriented at 0°, ±30°, and ±60° promotes a more uniform stress distribution under bending compared to progressive multiaxial configurations such as 5S (15,547 MPa).

For the carbon fiber series, the 2C architecture exhibits the highest flexural modulus, reaching 32,845 MPa, followed by 3C (30,478 MPa). These results emphasize the effectiveness of cross-ply and angle-ply configurations in maximizing bending stiffness by periodically aligning reinforcement along the principal loading directions and enhancing transverse constraint.

Elastic limit behavior

The energy at the elastic limit (Figure 2) reflects the ability of the laminate to store mechanical energy prior to the onset of non-linear deformation and damage initiation. In the glass fiber series, the values increase from 0.863 J for 1S to a maximum of 1.172 J for 4S, indicating an improvement in elastic deformation capacity with increasing angular dispersion. The 3S, 4S, and 5S architectures exhibit similar values, around 1.17 J, suggesting a saturation effect associated with progressive angular distributions.

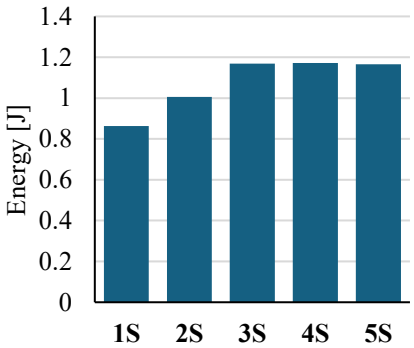

Figure 2 Energy at the elastic limit for glass fiber - reinforced composites as a function of laminate architecture.

In the carbon fiber series, the energy at the elastic limit ranges between 0.923 J (2C) and 1.175 J (3C). Despite the significantly higher stiffness of these laminates, the elastic energy storage remains comparable to that of the glass fiber composites, indicating a more rigid yet less elastically deformable response.

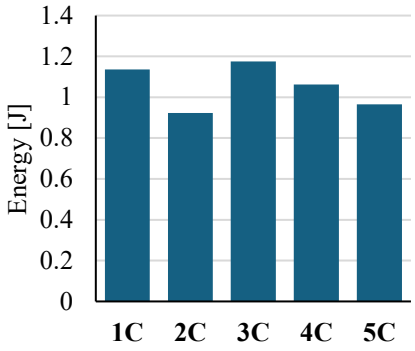

Figure 3 Energy at the elastic limit for carbon fiber-reinforced composites as a function of laminate architecture.

The load at the elastic limit (Figure 4) reveals pronounced differences between the two material families. For the glass fiber-reinforced laminates, the values range from 417 to 476 N, with the highest value observed for 3S (476 N). In contrast, the carbon fiber-reinforced laminates consistently exceed 800 N, reaching a maximum of 1,206 N for 3C, which reflects a substantially higher load-bearing capacity.

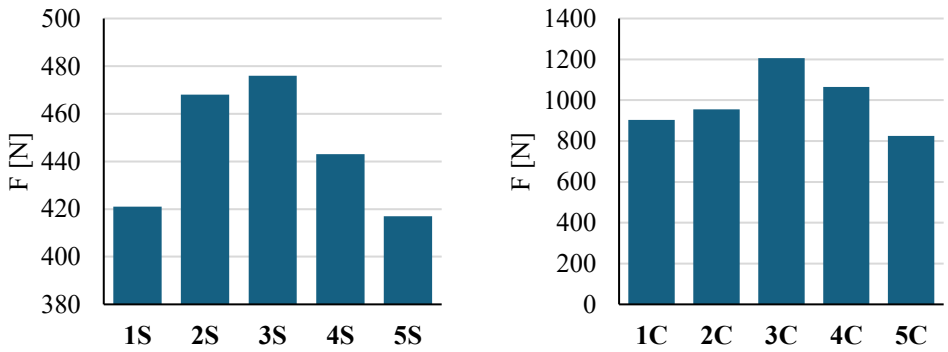

Figure 4 Load at the elastic limit for glass fiber- and carbon fiber-reinforced composites as a function of laminate architecture.

The stress at the elastic limit (Figure 4) follows a similar trend, with values between 349 and 422 MPa for the glass fiber series and between 386 and 582 MPa for the carbon fiber series. The highest elastic limit stress is recorded for 3C (582 MPa), indicating a significant delay in the onset of matrix microcracking and interlaminar damage under the combined effect of 0°, 90°, and ±45° ply orientations.

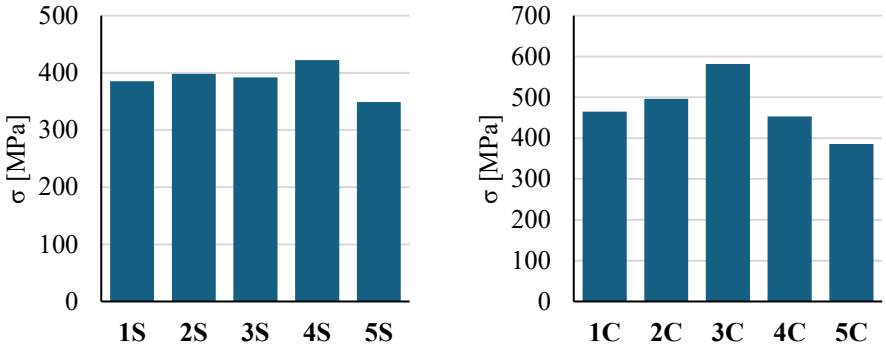

Figure 5 Stress at the elastic limit for glass fiber- and carbon fiber-reinforced composites as a function of laminate architecture.

Fracture behavior and energy absorption

The energy absorbed up to fracture (Figure 6) provides a measure of laminate toughness and its ability to dissipate mechanical energy prior to catastrophic failure. In the glass fiber series, the 5S architecture exhibits the highest fracture energy, reaching 1.712 J, followed by 4S (1.635 J). This behavior suggests that progressive multiaxial architectures promote gradual damage evolution mechanisms, such as matrix cracking, fiber–matrix debonding, and progressive interlaminar delamination.

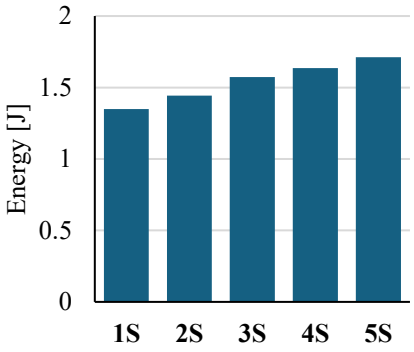

Figure 6 Energy at fracture for glass fiber - reinforced composites as a function of laminate architecture.

In the carbon fiber series, the highest fracture energy values are observed for 2C (1.792 J) and 3C (1.764 J), indicating that these architectures maintain a favorable balance between high stiffness and damage tolerance. However, compared to the glass fiber laminates, failure tends to be more localized and abrupt, which is characteristic of stiffer and stronger composite systems.

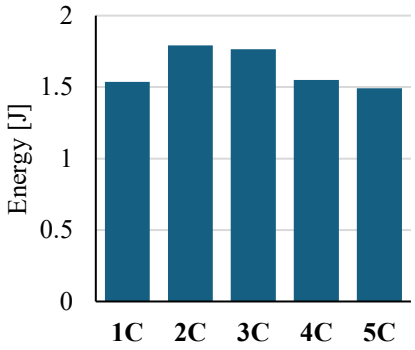

Figure 7 Energy at fracture for carbon fiber - reinforced composites as a function of laminate architecture.

The load at fracture (Figure 8) further highlights the structural advantage of carbon fiber-reinforced composites. Maximum values are achieved for 4C (572 N) and 5C (433 N), whereas for the glass fiber series the fracture loads remain below 220 N, with the highest value of 220 N for 4S.

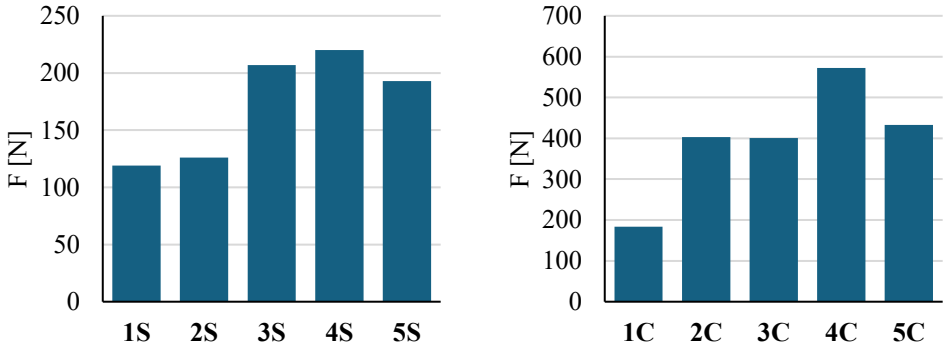

Figure 8 Load at fracture for glass fiber- and carbon fiber-reinforced composites as a function of laminate architecture.

The stress at fracture (Figure 9) shows a similar trend, with values ranging from 108 to 213 MPa for the glass fiber-reinforced composites and from 95 to 245 MPa for the carbon fiber-reinforced laminates. The maximum fracture stress is obtained for the 4C architecture (245 MPa), indicating enhanced resistance to crack propagation and final failure.

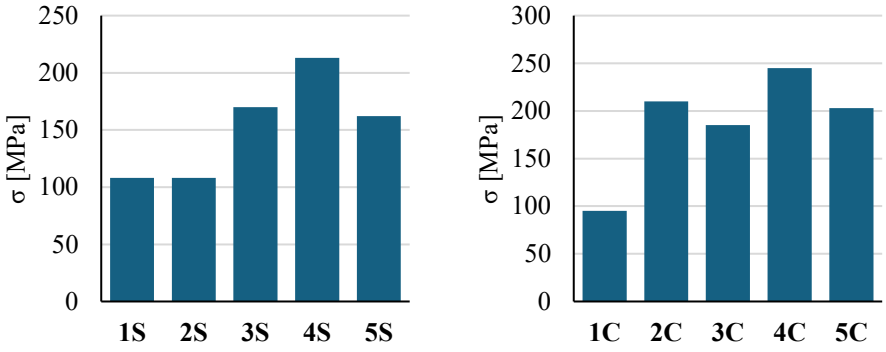

Figure 9 Stress at fracture for glass fiber- and carbon fiber-reinforced composites as a function of laminate architecture.

Correlation between laminate architecture and mechanical performance

The comparative analysis demonstrates that cross-ply and angle-ply architectures (2S, 2C, and 3C) maximize flexural stiffness and load-bearing capacity, whereas progressive multiaxial architectures (5S and 2C) favor energy absorption and damage tolerance. This relationship highlights an inherent trade-off between stiffness and toughness that can be effectively controlled through the design of the ply orientation sequence.

Furthermore, although variations in laminate thickness contribute to differences in bending moment of inertia, the experimental results indicate that architecture-induced effects dominate over thickness variations within each material family. This reinforces the role of ply orientation and stacking sequence as primary design parameters for tailoring flexural performance.

Design implications and structural applications

The findings suggest that laminate architecture can be strategically employed as a design variable to adapt the flexural response of epoxy-based textile-reinforced composites to specific application requirements. For structures where high stiffness and load-bearing capacity are critical, cross-ply and angle-ply configurations are recommended. Conversely, for applications demanding high energy absorption and damage tolerance, progressive multiaxial architectures offer superior performance.

Conclusions

Based on the results obtained from the three-point bending tests and the statistical processing of the experimental data, the present study highlights the decisive role of composite architecture and reinforcement type in controlling the mechanical behavior of epoxy-based textile-reinforced composites. The differences observed between the glass fiber-reinforced and carbon fiber-reinforced material series confirm the influence of the intrinsic properties of the fibers on the global stiffness of the structures, with flexural modulus values reaching maxima on the order of 32.8 GPa for optimized cross-ply and angle-ply architectures in carbon fiber systems, compared to a range of approximately 15–18 GPa for glass fiber-reinforced systems.

The analysis of the behavior at the elastic limit and at fracture shows that the stacking architecture influences not only the maximum level of the supported loads and stresses, but also the manner in which energy is stored and dissipated throughout the deformation and

failure process. Architectures characterized by discrete angular distributions, involving plies oriented at 0°, 90°, and ±45°, lead to high values of load and stress at the elastic limit, indicating enhanced efficiency of load transfer mechanisms and a delay in the onset of delamination. In contrast, composite specimens with more complex, progressive multiaxial architectures promote higher energy absorption up to fracture, as evidenced by the maximum fracture energy values obtained for the 5S and 2C configurations, which suggests the activation of gradual damage mechanisms such as matrix cracking, fiber–matrix debonding, and progressive interlaminar delamination.

A comparison of the mechanical performance within each material series indicates that variations in laminate thickness have a secondary effect on the flexural response relative to the orientation of the woven plies and the stacking sequence, with differences in stiffness, strength, and toughness being primarily correlated with the internal architecture of the structure. This result supports the notion that tailoring the ply orientation at different angles represents an effective design strategy for adjusting the trade-off between stiffness and energy absorption capacity according to the functional requirements of the intended application.

In this context, the correlations established between composite architecture and the measured mechanical parameters can be considered engineering-relevant and may serve as a basis for the development of design criteria aimed at optimizing the flexural performance of epoxy-based composites reinforced with glass and carbon fiber fabrics.

Bibliography

Al-Nadhari, A., Ulus, H., and Topal, S. 2025. Analyzing stiffness variations in 3D woven composites: A multi-instrumental study on glass/Kevlar hybridization effects under tensile and shear loads. Composites Part A, 191, 108722. https://doi.org/10.1016/j.compositesa.2025.108722

Bao, J., Wang, Y., An, R., Cheng, H., and Wang, F. 2022. Investigation of the mechanical and ballistic properties of hybrid carbon/aramid woven laminates. Defence Technology, 18(10), 1822–1833. https://doi.org/10.1016/j.dt.2021.09.009

Bergmann, T., Heimbs, S., and Maier, M. 2015. Mechanical properties and energy absorption capability of woven fabric composites under ±45° off-axis tension. Composite Structures, 125, 362–373. https://doi.org/10.1016/j.compstruct.2015.01.040

Bunea, M., Bria, V., Silva, F. S., Bîrsan, I. G., and Buciumeanu, M. 2021. Influence of fiber orientation and fillers on low velocity impact response of the fabric reinforced epoxy composites. Applied Composite Materials, 28(4), 1277–1290. https://doi.org/10.1007/s10443-021-09910-1

Capatina, A., Bria, V., Bunea, M., and Bîrsan, I.-G. 2019. Tensile behaviour of fabric reinforced laminates and plies. Materiale Plastice, 56(2), 370.

Gonabadi, H., Oila, A., Yadav, A., and Bull, S. 2022. Investigation of anisotropy effects in glass fibre reinforced polymer composites on tensile and shear properties using full-field strain measurement and finite element multi-scale techniques. Journal of Composite Materials, 56(3), 507–524. https://doi.org/10.1177/00219983211054232

Hu, D., Zhang, C., Ma, X., and Song, B. 2016. Effect of fiber orientation on energy absorption characteristics of glass cloth/epoxy composite tubes under axial quasi-static and

impact crushing condition. Composites Part A, 90, 489–501. https://doi.org/10.1016/j.compositesa.2016.08.017

Kostunin, D., Lasic, D. I., et al. 2016. Analysis of mechanical properties anisotropy of nanomodified carbon fibre-reinforced woven composites. IOP Conference Series: Materials Science and Engineering, 153(1), 012003. https://doi.org/10.1088/1757-899X/153/1/012003

Manohar, S., Samal, P., Dehury, J., and Paramita, P. 2020. Effect of fiber content and orientation on mechanical properties of epoxy composites reinforced with jute and Kevlar. Materials Today: Proceedings, 26, 273–277. https://doi.org/10.1016/j.matpr.2019.11.239

Sarasini, F., et al. 2013. Hybrid composites based on aramid and basalt woven fabrics: Impact damage modes and residual flexural properties. Materials & Design, 49, 290–302. https://doi.org/10.1016/j.matdes.2013.01.010

Ungureanu, C., and Bria, V. 2022. Effect of the fiber orientation of glass fiber reinforced polymer composites on mechanical properties. Annals of "Dunărea de Jos" University of Galați, Fascicle IX: Metallurgy and Materials Science, 40(2).

Yahaya, R., Sapuan, S. M., Jawaid, M., Leman, Z., and Zainudin, E. S. 2016. Effect of fibre orientations on the mechanical properties of kenaf–aramid hybrid composites for spall-liner application. Defence Technology, 12(1), 52–58. https://doi.org/10.1016/j.dt.2015.08.005

Zhou, G., et al. 2021. Experimental investigation on the effects of fabric architectures on mechanical and damage behaviors of carbon/epoxy woven composites. Composite Structures, 257, 113366. https://doi.org/10.1016/j.compstruct.2020.113366